CHEMISTRY OF MATERIALS

Article

pubs.acs.org/cm

Voltage Dependent Solid Electrolyte Interphase Formation in Silicon Electrodes: Monitoring the Formation of Organic Decomposition Products

Alison L. Michan, Michal Leskes, and Clare P. Grey*

Department of Chemistry, University of Cambridge, Lensfield Road, Cambridge, CB2 1EW, United Kingdom

Supporting Information

ABSTRACT: The solid electrolyte interphase (SEI) passivating layer that grows on all battery electrodes during cycling is critical to the long-term capacity retention of lithium-ion batteries. Yet, it is inherently difficult to study because of its nanoscale thickness, amorphous composite structure, and air sensitivity. Here, we employ an experimental strategy using ^{1}H, ^{7}Li, ^{19}F, and ^{13}C solid-state nuclear magnetic resonance (ssNMR) to gain insight into the decomposition products in the SEI formed on silicon electrodes, the uncontrolled growth of the SEI representing a major failure mechanism that prevents the practical use of silicon in lithium-ion batteries. The voltage dependent formation of the SEI is confirmed, with the SEI growth correlating with irreversible capacity. By studying both conductive carbon and mixed Si/C composite electrodes separately, a correlation with increased capacity loss of the composite system and the low-voltage silicon plateau is demonstrated. Using selective ^{13}C labeling, we detect decomposition products of the electrolyte solvents ethylene carbonate (EC) and dimethyl carbonate (DMC) independently. EC decomposition products are present in higher concentrations and are dominated by oligomer species. Lithium semicarbonates, lithium fluoride, and lithium carbonate products are also seen. Ab initio calculations have been carried out to aid in the assignment of NMR shifts. ssNMR applied to both rinsed and unrinsed electrodes show that the organics are easily rinsed away, suggesting that they are located on the outer layer of the SEI.

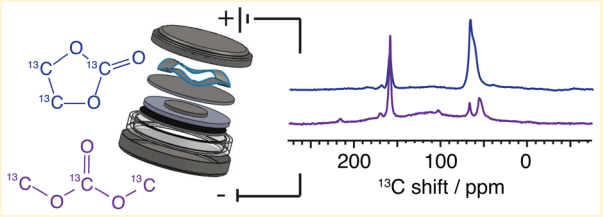

INTRODUCTION

The ability to cycle a Li-ion battery for multiple cycles requires that a stable solid electrolyte interphase (SEI) be formed on the electrodes. Without such a stable SEI, breakdown of the electrolyte continues unhindered, removing electrolyte (and lithium) from the cell. The SEI consists of both inorganic and organic species and represents an important interface within the cell with respect to Li^+ diffusion.[1−3] The relative amounts and types of decomposition products contained in the SEI depend on several factors including the electrolyte composition (1 M $LiPF_6$ in ethylene carbonate (EC) and dimethyl carbonate (DMC) in this study), formation conditions (i.e., current rate, temperature and voltage), and initial water content in the cell. It is also widely accepted that its composition and structure may be favorably controlled through the use of electrolyte additives. For example, additives such as fluoroethylene carbonate (FEC) and vinylene carbonate (VC) have been shown to increase capacity retention in Li-ion batteries. It is believed that they decompose into polymeric species, improving the stability of the SEI.[4−6]

The critical role of the SEI in capacity retention and battery failure drives the need for an improved understanding of the electrolyte decomposition products forming this interface on Li-ion battery electrodes. Due to its nanoscale thickness and composite nature, it is difficult to characterize. One strategy is to form as much SEI as possible in order to characterize its intrinsic structural and chemical properties. For example, reduction products of ethylene carbonate (EC) have been synthesized as model compounds.[7−9] Here, we focus on the SEI formation in a crystalline powder Si system mixed with conductive C to identify many of the SEI components. The continual and essentially unimpeded growth of SEI on Si is perhaps the most important failure mode of Si anodes, which provides a strong motivation for the study of this particular system.[10]

The use of Si as an anode material should in principle result in significant improvements in energy density in Li-ion batteries: the theoretical gravimetric capacity of Si (3579 $mAhg^{-1}$ based on $Li_{15}Si_4$) being 10 times that of the most commonly used anode material in commercially available Li-ion batteries, graphite (372 $mAhg^{-1}$).[11,12] However, insufficient capacity retention in Si systems limits their widespread use. Si has a large volume expansion (300%) on lithiation that is thought to contribute toward the formation of a thick and unstable SEI. Cracking in the SEI due to mechanical strains may expose fresh surfaces which leads to further SEI formation. It is therefore desirable to design a stable (flexible) SEI layer on the surfaces of Si particles. The use of additives in these systems has successfully improved capacity retention and may partially satisfy this requirement.[13] In addition, an electrochemical

Received: November 11, 2015
Revised: November 19, 2015
Published: November 20, 2015

DOI: 10.1021/acs.chemmater.5b04408
Chem. Mater. 2016, 28, 385−398

cycling strategy of limiting the discharge capacity in these systems can also improve capacity retention.[11,14] A more detailed understanding of the SEI formed on this material and its voltage dependence may allow for a more fundamental approach to the problem of designing a stable SEI.

Previously detected and predicted SEI decomposition products in EC/DMC systems include LiF, LiOH, Li_2CO_3, $ROCO_2Li$, ROLi, and poly(ethylene oxides) PEO.[1,7,15−21] Si-specific SEI studies have detected SiO_xF_y species on the surfaces of Si showing that the SEI on Si may differ from graphitic systems.[22] The effects of ambient exposure and sample preparation on detected chemical species in SEI studies have been investigated.[17,18,23] These studies have explored the sensitivity and solubility of the SEI, showing a need for careful anoxic studies and further exploration of the solubility of SEI products. Li^+ transport through the SEI layer has been investigated by Lu and Harris.[24] They found that electrolyte diffused into a porous surface region; underneath, they detected a more tightly packed region containing Li_2O and/or Li_2CO_3. In a related study, a mechanism for Li^+ transport through the SEI is presented.[25] Borodin et al.[26] have used molecular dynamics to predict how Li^+ may be coordinated to the semicarbonate decomposition products of EC, which form conductive pathways for Li^+ diffusion.

In our investigation, we use solid-state NMR (ssNMR) to monitor electrolyte decomposition as a function of voltage on the first electrochemical cycle. We make extensive use of ^{13}C-labeled electrolytes using fully labeled EC and DMC electrolyte solvents, together with a ^1H, ^{19}F, ^7Li, and ^{13}C ssNMR multinuclear study, in an attempt to comprehensively characterize the local environments of the SEI. Previous ssNMR studies of the SEI formed in graphitic and Si systems have only used selective labeling on a single carbonate site of EC.[27,28] The fully labeled electrolytes used in this study reveal additional organic environments including oligomer species. A binder-free Si electrode is used here to remove the variable of commonly used binders such as carboxymethylcellulose (CMC) used in electrode formulation, which may also inhibit SEI growth.[12,29−33] Additionally, the small particle size of the 50 nm crystalline powder used in this study provides a large surface area for SEI formation. Selective ^{13}C-labeling of the electrolytes is used to follow EC and DMC decomposition mechanisms independently and determine relative quantities of their decomposition products. Correlation spectroscopy is used to characterize organic products and Li^+ coordination in carbonate environments relevant to Li^+ transport through the SEI layer. ^7Li and ^{13}C chemical shifts in semicarbonates are investigated using ab initio calculations to aid the spectral assignments. Finally, our electrochemistry shows SEI forming on the conductive C in the system independently of Si.

EXPERIMENTAL METHODS

Enriched Electrolyte Preparation. Enriched electrolytes were prepared by dissolving 1 M lithium hexafluorophosphate $LiPF_6$ (Sigma-Aldrich) in ethylene carbonate (EC) and dimethyl carbonate (DMC) 1:1 w/w. 25% ^{13}C enriched electrolytes were prepared with either carbonate enriched ^{13}C EC denoted $^{13}C_1$ EC, fully labeled $^{13}C_3$ EC, or fully labeled $^{13}C_3$ DMC (Figure 1). $^{13}C_1$ EC (Icon) and $^{13}C_3$ EC (Sigma-Aldrich) were dried under vacuum in a mini-desiccator and transferred to an Ar glovebox. ^{13}C DMC (Sigma-Aldrich) was dried using 4 Å molecular sieves and transferred to an Ar glovebox. Nonlabeled battery grade EC (Sigma-Aldrich) and DMC (Sigma-Aldrich) were used to dilute the 99% enriched carbonates. Battery

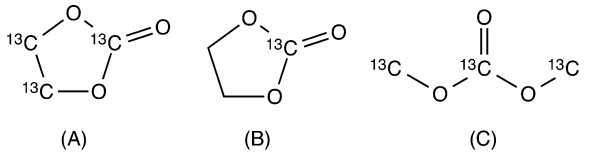

Figure 1. Selectively enriched (A) $^{13}C_3$ EC, (B) $^{13}C_1$ EC, and (C) $^{13}C_3$ DMC electrolyte molecules.

grade LP30 (1 M $LiPF_6$ in EC/DMC 1:1 w/w by BASF) was used when no isotope enrichment was required.

Electrochemical Cycling. 50 nm Si powder (Sigma-Aldrich) was ball-milled with Carbon SuperP (Timcal) using two 1/2 in. diameter balls in a 70 mL stainless steel ball mill jar for 10 min to evenly mix the two powders. The C/Si mixture was then dried on a vacuum line at 100 °C for 2 days to remove water from the system and then transferred to an Ar glovebox. The C/Si 1:1 w/w powder electrode samples were prepared in 2032 coin cells against 13 mm diameter Li metal electrodes in an Ar glovebox (typically O_2 < 0.1 ppm and H_2O < 0.1 ppm). Typical powder masses in coin cells were 1 to 3 mg. Standard porous glass fiber mat separators (Whatman GF/B, 1 mm thick) were saturated with electrolyte. In the preparation of the ^{13}C enriched coin cells, an additional Celgard 2340 separator layer was used against the electrode surface to avoid any glass fiber sticking to the surface of the powder samples. The separators and coin cell parts were dried in a 60 °C oven overnight (minimum) to remove excess water before being transferred to the Ar glovebox.

Coin cells were galvanostatically cycled (using an Arbin Instruments or Biologic VSP) at a current rate of C/X (X = 75 h) calculated by

$$I = C_{Si} m_{Si} X^{-1} \quad (1)$$

with C_{Si} based on the theoretical capacity of 3579 $mAhg^{-1}$ for crystalline $Li_{15}Si_4$ and m_{Si}, the mass of Si in the electrode. After cycling, the coin cells were disassembled under Ar and dried under dynamic vacuum in the prechamber of the glovebox overnight. No solvent was used to rinse excess electrolyte from the samples to avoid any structural or compositional change to SEI grown on the electrode surfaces. The electrochemical data were processed using Biologic EC-Lab V10.34 and MATLAB software. Carbon SuperP powder coin cells were prepared using the same method as described for the combined C/Si powder samples. The powder was dried on a vacuum line overnight and transferred to an Ar glovebox. The cells were galvanostatically cycled at an equivalent current density to C/75 in the C/Si system. As the C/Si mixture is combined in a 1:1 ratio and the C/Si system current rate is based on the active mass of Si, an equivalent current density to C/X (X = 75 h) is easily calculated by

$$I = C_{Si} m_C X^{-1} \quad (2)$$

with C_{Si} based on the theoretical capacity of Si (3579 $mAhg^{-1}$) and m_C being the mass of carbon (equal to m_{Si} in the C/Si electrodes).

Solid-State NMR. Ex situ multinuclear ssNMR spectra were obtained on 16.4 T Bruker Avance III 700 MHz and 9.4 T Bruker Avance 400 MHz spectrometers. Samples were packed under Ar, avoiding any exposure to ambient air, into rotors of 1.3, 3.2, and 4 mm outer diameters. Magic-angle spinning (MAS) frequencies ranged from 10 to 60 kHz, spinning under N_2. Several electrode samples (of 1 to 3 mg) were combined in the larger 3.2 and 4 mm diameter rotors to fill the rotors and enhance signal in the experiments. ^1H and ^{13}C chemical shifts were externally referenced to adamantane (^1H 1.9 ppm, ^{13}C 38.5 ppm) and ^7Li and ^{19}F to LiF (−1 ppm, −204 ppm, respectively). The data were processed using Bruker TOPSPIN software and analyzed using dmfit software.[34] Typical radio frequency (RF) field strengths used were 90−125 kHz, for ^1H, ^7Li, ^{19}F, and ^{13}C, respectively.

Nonlabeled electrode samples were cycled as a function of voltage and investigated using ^1H ssNMR Hahn echo experiments. Multinuclear ssNMR measurements were performed on one sample cycled between 1 mV and 2 V. Samples prepared with each of the ^{13}C-labeled electrolyte solvents (A, B, C, Figure 1) were investigated by direct excitation ^{13}C ssNMR experiments to obtain relative quantitative

DOI: 10.1021/acs.chemmater.5b04408
Chem. Mater. 2016, 28, 385−398

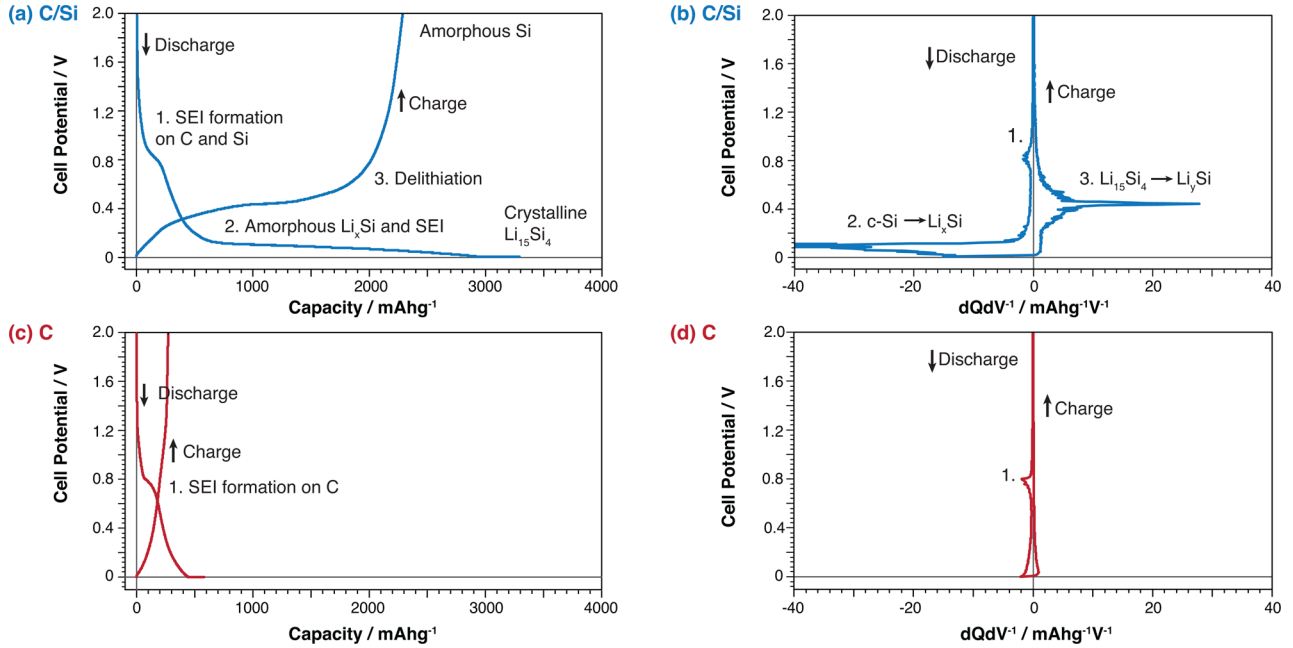

Figure 2. First electrochemical cycle of a C/Si electrode galvanostatically cycled against Li metal and plotted as a function of (a) capacity per g of Si and (b) differential capacity $dQdV^{-1}$. The C SuperP cell was galvanostatically cycled (at an equivalent current rate to a C/Si electrode based on the theoretical capacity of Si) and plotted as a function of (c) capacity per g and (d) differential capacity. Key electrochemical processes are labeled 1−3, with Si processes clearly absent in the C-only sample. c-Si indicates crystalline Si.

information on chemical environments. $^{1}H-^{13}C$ and $^{7}Li-^{13}C$ cross-polarization (CP) experiments were used to detect local environments with these nuclei in close spatial proximity by transferring magnetization from ^{1}H and ^{7}Li nuclei to ^{13}C nuclei. Two-dimensional (2D) $^{1}H-^{13}C$ heteronuclear correlation (HETCOR) experiments were performed on each of the labeled-sample types (A, B, C). The ^{13}C spectra were typically acquired using swept-frequency two-pulse phase modulation (swfTPPM)[35] ^{1}H decoupling at 80 kHz. A ^{13}C direct excitation homonuclear Radio Frequency Driven Recoupling (RFDR)[36] correlation experiment was performed on the $^{13}C_3$ EC sample (A) only. Finally, an experiment was performed to investigate the effects of rinsing the samples using nonlabeled DMC: quantitative direct excitation ^{13}C experiments were performed before and after rinsing. Sample preparation has also been extensively investigated in previous SEI studies.[17,18,23] Further experimental details are given in the Supporting Information.

COMPUTATIONAL METHODS

Chemical shifts were calculated using Density Function Theory (DFT) using Gaussian 09[37] (all molecules in gas phase) and simulated using ChemNMR, included within ChemBioDraw 13.0. ChemNMR approximates ^{13}C and ^{1}H chemical shifts with respect to TMS. For all DFT calculations, the hybrid functional B3LYP[38,39] and 6-311G++(d,p) basis set[40,41] was used, in combination with tight convergence. Frequency calculations were performed to confirm ground state convergence. The absolute NMR shift values were referenced to adamantane and LiF for ^{13}C, ^{1}H, ^{7}Li, and ^{19}F, respectively, as in the experiment.

Simulated fits of the experimental ^{13}C spectra were performed in dmfit[34] to provide an approximation of the relative abundance of chemical environments and support ssNMR assignments. The simulation fit amplitudes were converged to within 10% error, with peak widths and positions constrained and supported by cross-polarization and correlation experiments. The large- and small-amplitude resonances were converged separately.

RESULTS

Electrochemical Analysis of the First Cycle. First, we examine the electrochemistry in the first cycle of both C/Si composite and C SuperP (only) powder cells. Figure 2 presents the voltage versus net capacity and differential capacity curve of the coin cells cycled between 1 mV and 2 V vs Li metal. Any deviation of the capacity from that of the theoretical capacity of Si (3579 $mAhg^{-1}$) of the binder-free cells is ascribed to electrically inactive material in the cells (therefore, a reduced mass of Si), mass errors, or additional capacity arising from SEI formation.[42] As can be seen in the differential curve, there is an electrochemical process near 0.8 V, thought to correspond to SEI formation on the C and/or Si surfaces. The plateau in the region of 0.15 V is characteristic of the lithiation of crystalline Si and formation of amorphous Li_xSi phases.[11,14,42,43] At the bottom of the discharge, the C/Si powder was held at 1 mV for 12 h to lithiate more of the Si, and additional capacity was observed. The voltage of the plateau on charge/delithiation (process 3, Figure 2b) is characteristic of the delithiation of $Li_{15}Si_4$ confirming that this crystalline phase was formed on discharge. In the final stage of cycling, the cell is held at 2 V to fully delithiate the amorphous Si. The capacity loss represented by the difference in discharge and charge capacity is thought to result from a combination of poor electrical connectivity and SEI formation on the C and Si particle surfaces. To independently observe the electrochemistry of the conductive carbon, a C SuperP coin cell was cycled at an equivalent current density to the C/Si system (approximately 48 mAg^{-1} of C), and the differential curve shows the process near 0.8 V occurs in the C SuperP system while the Si processes are absent as expected. A capacity approaching 580 $mAhg^{-1}$ is obtained, showing a portion of the initial discharge and irreversible capacity observed in the first cycle of the C/Si electrode system is observed on C rather than Si. However, a much greater irreversible capacity is seen in the C/Si system.

DOI: 10.1021/acs.chemmater.5b04408
Chem. Mater. 2016, 28, 385−398

Investigation of SEI Formation as a Function of Voltage. To investigate SEI formation as a function of voltage, several samples were held at decreasing low cutoff voltages, Figure 3a. The cells were then charged and delithiated at a cell

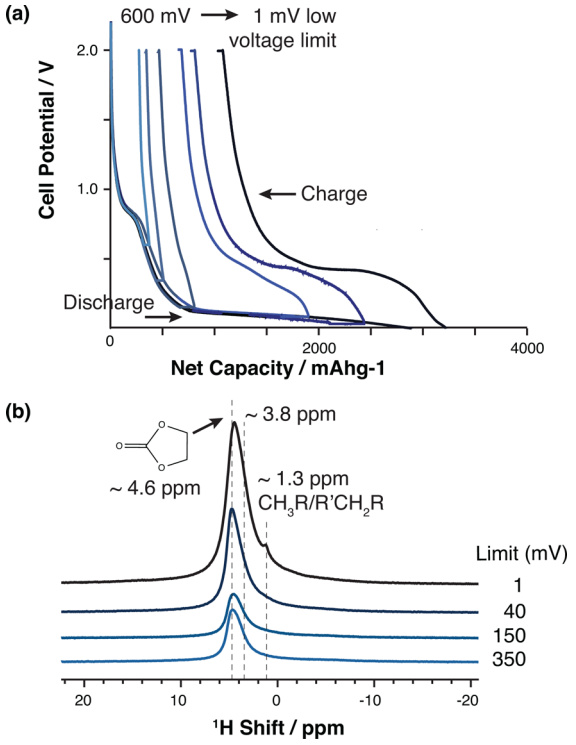

Figure 3. (a) The electrochemical profiles of C/Si coin cells cycled to decreasing low voltage limits and charged to 2 V. (b) ^{1}H Hahn echo ssNMR spectra of the unrinsed C/Si electrode samples, with their corresponding voltage limits indicated. The spectra were acquired with 60 kHz MAS and are scaled by their mass. Residual EC and mass error due to separator material adhering to electrode surfaces leads to some quantitative variation in the spectra.

potential of 2.0 V. The electrode samples were investigated by ssNMR without rinsing to avoid any possible dissolution of the SEI components and consequent compositional changes. As a consequence, the ^{1}H spectra contain some residual EC at 4.6 ppm Figure 3b. A resonance at approximately 1.3 ppm and shoulder at 3.8 ppm are also observed (seen more clearly in Figure 4). While these resonances overlap with each other making accurate deconvolution to extract relative intensities difficult, it is clear that the overall intensity of the ^{1}H NMR signals (in Figure 3b) correlate with the capacity loss observed in Figure 3a. The resonance at 1.3 ppm is resolved below 40 mV and is assigned to a CH_3R or $R'CH_2R$ group. The increased capacity loss and formation of new chemical environments that occur during the low voltage plateau (Figure 2a, process 2) demonstrate how the Si electrochemistry and cycling voltage limits dictate SEI formation in these systems.

To confirm the assignment for the residual EC in the system (and negligible DMC), control ^{13}C and ^{1}H experiments were performed on an uncycled electrode sample (Supporting Information). The dried pristine sample, before cell assembly, contained some trace amount of water resonating at 4.5 ppm (^{1}H). By soaking the uncycled sample with electrolyte, residual EC in the sample was confirmed to resonate at approximately (^{1}H) 4.6 ppm and (^{13}C) 160 and 67 ppm.

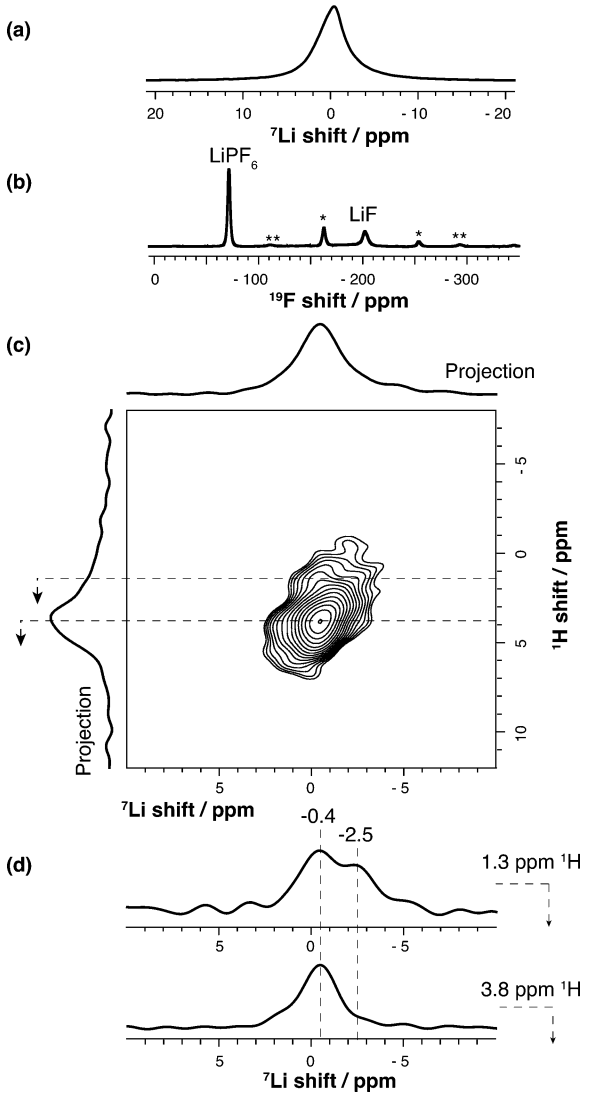

Figure 4. Unrinsed C/Si electrode sample discharged to a 1 mV limit was investigated using (a) ^{7}Li single-pulse, (b) ^{19}F Hahn echo, and (c) ^{1}H−^{7}Li heteronuclear correlation ssNMR experiments. Slices of the 2D spectrum are shown in (d). The correlation spectrum was acquired using a CP contact time of 4 ms to transfer magnetization from ^{1}H to ^{7}Li. Spinning sidebands are indicated with (*) $LiPF_6$ and (**) LiF.

The sample discharged to the lowest voltage limit of 1 mV (Figure 3a) was further investigated by multinuclear ssNMR using a combination of ^{1}H, ^{7}Li, ^{19}F one dimensional (1D) and ^{1}H−^{7}Li ssNMR correlation experiments (Figure 4). The broad ^{7}Li spectrum indicates a superposition of several Li environments with similar chemical shifts, including residual $LiPF_6$ and lithium salts in the SEI such as lithium carbonate.[44] The ^{19}F spectrum confirms the presence of $LiPF_6$. LiF is the only other species detected, present in a relatively low amount compared to $LiPF_6$. No additional resonances relating to the decomposition of $LiPF_6$ were identified in the ^{19}F spectra. Two dimensional (2D) correlation experiments were performed to resolve the different ^{1}H-containing species (Figure 4c). The ^{1}H dimension in the 2D ^{1}H−^{7}Li correlation spectrum is dominated by a broad ^{1}H resonance at 3.8 ppm, which correlates with a broad ^{7}Li resonance with a shift of approximately −0.4 ppm (Figure 4d). A slice of the ^{1}H−^{7}Li 2D spectrum at a ^{1}H shift of 1.3 ppm reveals that the 1.3 ppm signal is correlated to ^{7}Li

DOI: 10.1021/acs.chemmater.5b04408
Chem. Mater. 2016, 28, 385−398

Table 1. Predicted SEI Decomposition Products and Their Tabulated ^{13}C, ^{1}H, and ^{7}Li Chemical Shifts[a]

Molecule	Atom	Calculated and Measured Chemical Shifts / ppm ChemNMR	DFT	Experimental
LEDC				(solvent: AC-d_6[9]/D_2O[7])
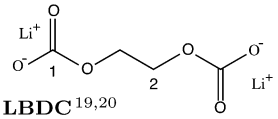	C1	161	171.0	157/161.2
	C2	65.5	64.5	62.9/62.5
	H2	4.39	4.3	3.53/3.51
	Li	-	0.9	
LBDC[19,20]				
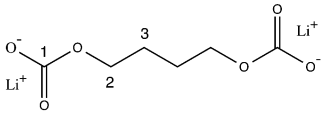	C1	161	171.3	
	C2	67.1	68.0	
	C3	24.8	25.4	
	H2	4.21	4.1	
	H3	1.61	1.7	
	Li	-	1.0	
LEC				(solvent: D_2O[8])
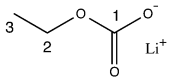	C1	161	171.4	163.7
	C2	63.5	62.8	60.1
	C3	13.8	11.9	19.4
	H2	4.21	4.1	3.65
	H3	1.27	1.5	1.17
	Li	-	1.0	
LMC				(solvent: AC-d_6/DMSO[9]/D_2O[8])
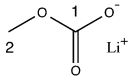	C1	161	171.9	160.97/157.02/163.1
	C2	54.1	51.5	62.40/51.51/54.6
	H2	3.68	3.8	3.56/3.27/3.35
	Li	-	0.9	na
PEO				
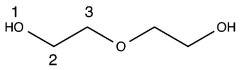	C2	61.3	62.5	
	C3	70.3	70.9	
	H1	5.4	0.1	
	H2	3.7	4.0	
	H3	3.54	3.7	

[a]A more complete table is included in the Supporting Information.

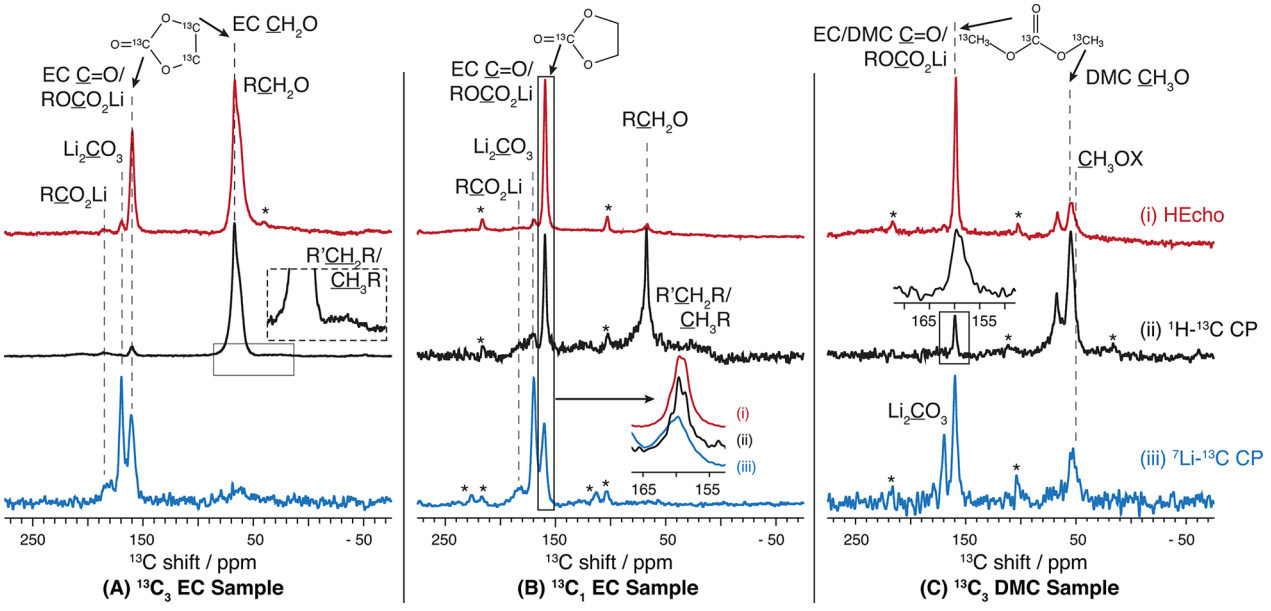

Figure 5. NMR spectra of Si anodes extracted from coin cells cycled using (A) $^{13}C_3$ EC, (B) $^{13}C_1$ EC, and (C) $^{13}C_3$ DMC labeled electrolytes. The electrode samples were probed using a combination of (i) ^{1}H Hahn echo (HEcho), (ii) $^{1}H-^{13}C$ CP with a short contact time of 500 μs to transfer magnetization from ^{1}H to ^{13}C, and (iii) $^{7}Li-^{13}C$ CP with a long contact time of 5000 μs to transfer magnetization from ^{7}Li to ^{13}C. The spectra of sample A were acquired with 12 kHz MAS rate and samples B and C with 10 kHz MAS rate. Spectra are scaled by maximum signal intensity and are not quantitatively comparable.

signals near −0.4 and −2.5 ppm (Figure 4d). The −0.4 ppm resonance is due to a lithium salt, presumably in the SEI,[44] while the −2.5 ppm signal is assigned to $LiPF_6$ based on an independent ssNMR measurement of the neat $LiPF_6$ salt. The correlation between the ^{1}H resonance at 1.3 ppm and the ^{7}Li species is weaker than the correlation seen for the 3.8 ppm resonance, and as a result, the 1.3 ppm signal is barely visible in the ^{1}H projection (see the ^{1}H axis of the 2D spectrum). A close proximity to $LiPF_6$ in these unrinsed samples suggests either a porous SEI structure or product formed on an outer layer of the SEI near the electrolyte. These assignments are further explored using ^{13}C labeled electrolytes.

DOI: 10.1021/acs.chemmater.5b04408
Chem. Mater. 2016, 28, 385−398

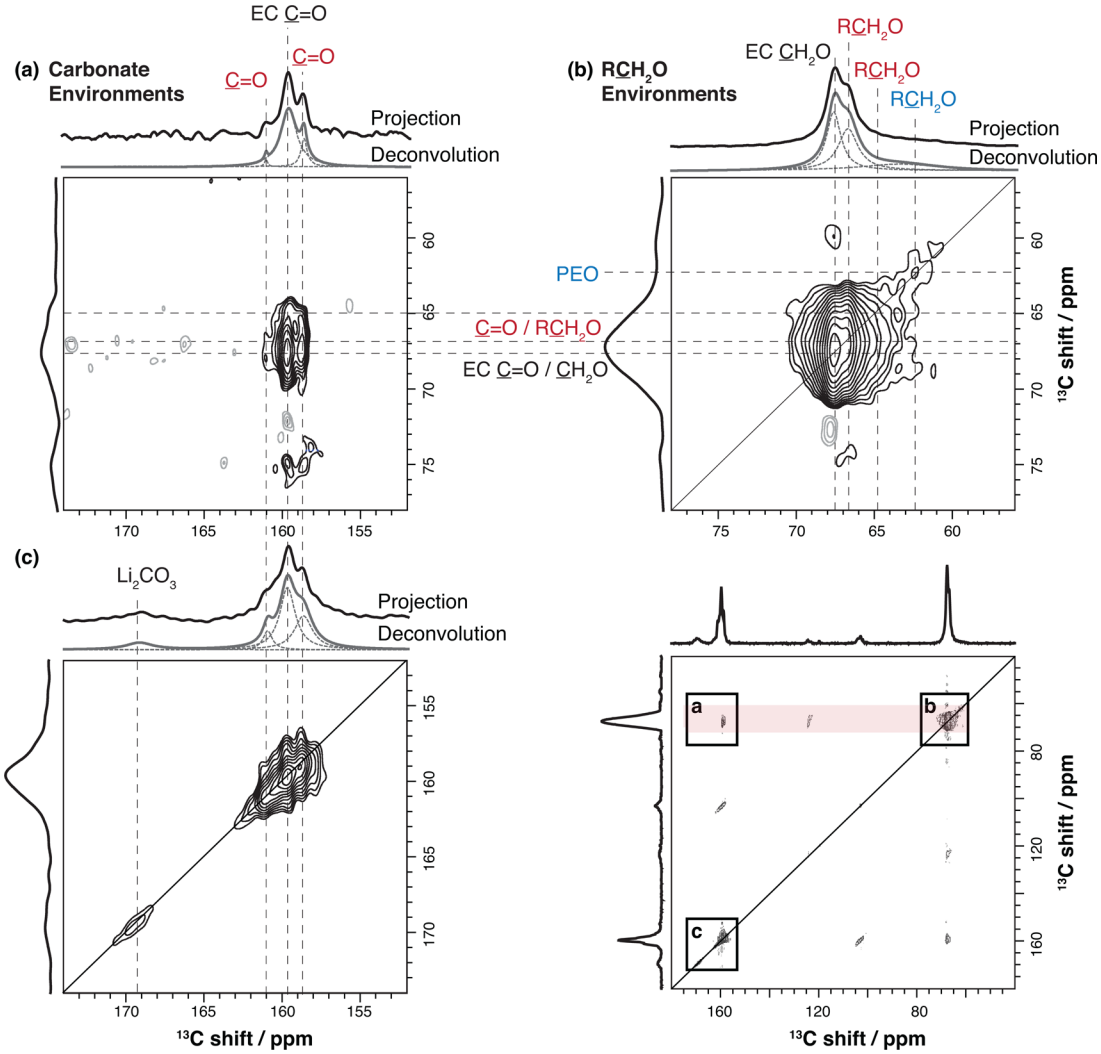

Figure 6. $^{13}C-^{13}C$ Homonuclear correlation experiment of a sample prepared with $^{13}C_3$ EC labeled electrolyte. The spectrum was acquired on a 700 MHz spectrometer with a 10 kHz MAS rate and an RFDR mixing time of 5 ms. Panel (a) shows the cross peaks between resonances in (b) and (c). Correlating and noncorrelating resonances are indicated in red and blue, respectively. Summed projections of the ranges shown and their deconvolutions are presented in each panel (a, b, c).

^{13}C-Labeled Samples. Coin cells were prepared with selectively enriched electrolytes, and the samples were investigated using a combination of 1D and 2D ssNMR techniques. In order to interpret the spectra and aid our assignment, we have considered many of the possible organic molecules and salts that have been proposed to result from decomposition of the electrolyte. The ^{13}C and ^{1}H shifts of these species are presented in Tables 1 and S1, where the shifts have been determined either from prior studies, ssNMR reference measurements of model compounds, DFT calculations, or ChemNMR simulations. Although distinct chemical shift ranges are observed for the various local environments within the different possible SEI components, noticeable differences are observed between the calculated (DFT), estimated (ChemNMR), and experimentally determined solution NMR values. The variations are ascribed to the limitations of the approach (e.g., the DFT calculations were performed for molecules in the gas phase), coupled with the inherent difficulty in accounting for differences in solvation and packing effects in these disordered systems. Furthermore, it is not obvious how to appropriately include H-bonding and interactions with the Li^+ ions, without more detailed structural information.

1-Dimensional Experiments. Figure 5 shows a direct comparison between the three different selectively enriched samples (A, B, C; see Figure 1) following one electrochemical cycle. The ^{13}C Hahn echo spectra (Figure 5-i) provide information about the relative amounts of species detected in the (158−190 ppm) carbonate and carboxyl region and the (62−67 ppm) $-CH_2-$ regions. The signal contribution at ∼67 ppm in the $^{13}C_3$ EC Sample (A-i) is large compared with the $^{13}C_1$ EC Sample (B-i) due to the enrichment of the CH_2 groups of EC. In contrast, the $^{13}C_3$ DMC Sample (C-i) shows a weak signal contribution at ∼67 ppm resulting from natural abundance EC, in addition to a detectable signal at ∼55 ppm due to enriched DMC and its associated decomposition products. The $^{1}H-^{13}C$ and $^{7}Li-^{13}C$ cross-polarization (CP) experiments are used to identify groups of chemical environments in close spatial proximity, with these assignments later supported using 2D experiments. Overlapping carbonate resonances, indicated by a non-Lorentzian line shape, are shown in detail for Sample B (Inset in B-iii (spectra i, ii, iii)) and Sample C (Inset in C-ii). Broad line widths in the ssNMR

DOI: 10.1021/acs.chemmater.5b04408
Chem. Mater. 2016, 28, 385−398

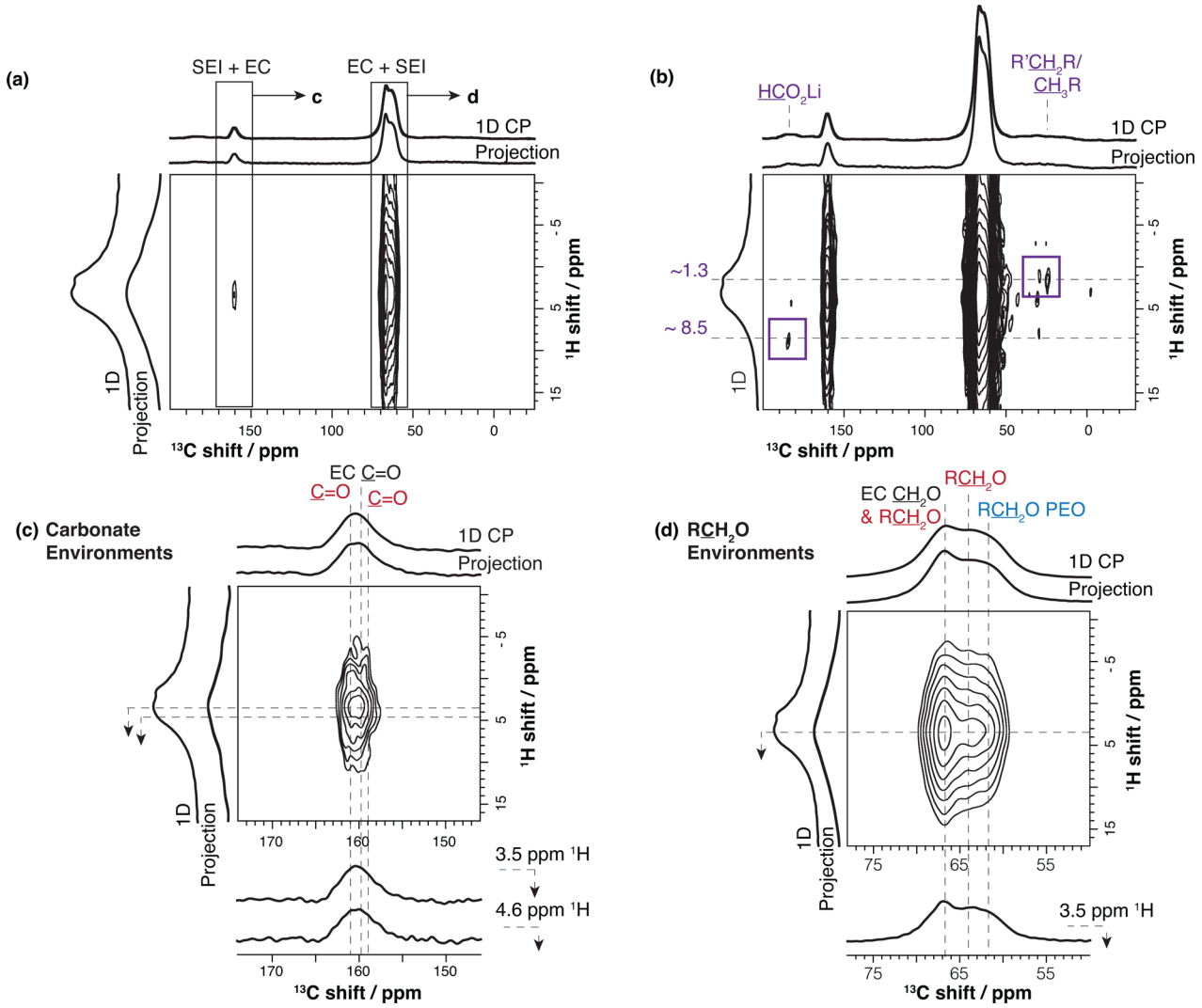

Figure 7. ^{1}H−^{13}C Heteronuclear correlation of a sample prepared with $^{13}C_3$ EC labeled electrolyte. The spectrum overview of panel (a) is presented with more contour levels in panel (b) to show evidence of ^{1}H correlations (purple). Panels (c) and (d) show enlargements of the carbonate and CH_2 regions of the ^{13}C spectrum, with the resonances labeled in red and blue corresponding to Figure 6. The spectrum was acquired on a 400 MHz spectrometer with 12 kHz MAS rate and contact time of 1000 μs to transfer magnetization from ^{1}H to ^{13}C.

spectra (including inset A-ii) largely arise from distributions of chemical shifts, typical of amorphous environments.

The ^{1}H−^{13}C CP spectra (Figure 5-ii) confirm at least three overlapping 161−159 ppm resonances that include residual EC solvent (160 ppm) and decomposition products containing a carbonate group (see inset B-iii, black (ii)). In the labeled-DMC Sample C, similar overlapping resonances are observed, with natural abundance EC and its associated decomposition products contributing significantly, and the majority of DMC is removed in the drying process during sample preparation. In each of the ^{13}C-labeled EC samples (A, B), a broad resonance extending from 0 to 50 ppm, centered at approximately 25−30 ppm, is observed. The very broad resonance indicates the presence of amorphous environments and is consistent with carbon environments such as $\underline{C}H_3CH_2O-$ and/or $-CH_2\underline{C}H_2CH_2-$ (the observed ^{13}C nuclei are underlined). This broad resonance is only visible in the $^{13}C_3$ EC Sample direct excitation spectrum (A-i) suggesting a more significant contribution from environments formed by the decomposition of EC. Its relatively low contribution in (A-ii) may be a result of the differences in the CP efficiency: (A-ii) was obtained at a lower field and under different experimental conditions than (B-ii) and (C-ii) or a dynamic range limitation in the presence of the dominant RCH_2O signal. The spectrum of the $^{13}C_3$ DMC Sample (C-ii) reveals a signal at ~56 ppm and shoulder at ~53 ppm (in addition to natural abundance EC and associated decomposition products at ~67 ppm). Some signal contribution is assigned to residual labeled-DMC, and the dominant shoulder is assigned to $\underline{C}H_3OX$.

The ^{7}Li−^{13}C CP spectra of all the samples (Figure 5-iii) reveal Li containing environments assigned to $R\underline{C}O_2Li$ (~185 ppm) and $Li_2\underline{C}O_3$ (~170 ppm). The 161 ppm resonance (see inset B-iii, blue) is strongly enhanced in the ^{7}Li−^{13}C cross-polarization experiment, suggesting that the corresponding environment is in closer spatial proximity to ^{7}Li than EC (~160 ppm) and is likely an $ROCO_2Li$ decomposition product. In addition, in the $^{13}C_3$ DMC Sample (C-iii), an environment at ~52−55 ppm is detected which can be assigned to a CH_3OX species most likely containing or nearby Li. The carboxylate (RCO_2Li) resonance is barely visible in the DMC-labeled sample (C-iii) and is not detectable by direct excitation (C-i)

DOI: 10.1021/acs.chemmater.5b04408
Chem. Mater. 2016, 28, 385−398

suggesting a more significant contribution from environments formed by the decomposition of EC.

2-Dimensional Correlation Experiments. A ^{13}C homonuclear correlation experiment was performed on the sample prepared with $^{13}C_3$ EC (Sample A) to detect carbons in close spatial proximity, Figure 6. As the spectrum has a low signal-to-noise ratio and is partially truncated in the indirect (vertical) dimension (due to time constraints in the spectral acquisition), the chemical shifts are interpreted with some margin of error on the order of ±0.5 and ±1.0 ppm in the horizontal and vertical dimensions, respectively. The off-diagonal region in Figure 6a shows carbonate environments correlating with R$\underline{C}H_2O$− groups (65−68 ppm, indicated in red) confirming multiple overlapping carbonate resonances and showing evidence for semicarbonate SEI products. Examining the carbonate peaks (of Figure 6a) from left to right, a minor carbonate environment at ∼161 ppm, visible in the sum projection and in Figure 6c, weakly correlates with the R$\underline{C}H_2O$ environment at ∼67 ppm. This correlation likely indicates an $\underline{R}O\underline{C}O_2Li$ SEI decomposition product. The second, and most dominant, carbonate peak at ∼160 ppm that correlates with the ∼67.5 ppm resonance is assigned to labeled EC. The carbonate resonance at ∼159 ppm correlates with at least two R$\underline{C}H_2O$ resonances at ∼65 and ∼67 ppm. This ∼159 ppm carbonate resonance likely indicates another $RO\underline{C}O_2Li$ SEI decomposition product. The correlation to at least two different R$\underline{C}H_2O$− resonances in the range of 65−68 ppm indicates close spatial proximity to at least one SEI decomposition product containing an R$\underline{C}H_2O$− group. While we have assigned the ∼159 and ∼161 ppm resonances to electrolyte decomposition products, we cannot completely exclude the possibility that different packing arrangements of EC with the SEI may result in differences in chemical shifts. R$\underline{C}H_2O$− resonances that do not correlate with carbonate groups (61−65 ppm, indicated in blue) suggest the presence of PEO-type oligomers $(-CH_2-CH_2-O-)_n$. Lastly, the $Li_2\underline{C}O_3$ resonance (Figure 6c) does not correlate with any other carbon species (Figure 6a), as expected.

2D $^1H-^{13}C$ correlation experiments were performed on the three labeled samples, Figures 7, 8, and 9, with full spectra presented in the Supporting Information. For the sample prepared with $^{13}C_3$ EC, Figure 7b shows broad peaks in the cross-polarization experiment that correlate weakly with ^1H resonances, consistent with amorphous phases and distributions of chemical environments. A weak ^1H resonance at approximately 8.5 ppm correlating with a carboxyl ^{13}C resonance at 185 ppm indicates some lithium formate $H\underline{C}O_2Li$ may be present. The weak correlation observed for this resonance (compared to its contribution in the 1D spectrum in Figure 5) suggests that additional RCO_2Li species (with R ≠ H) may be present. The ^1H resonance at approximately ∼1.3 ppm has a very weak correlation with the broad ^{13}C resonances at ∼25−30 ppm, consistent with assignments to $\underline{C}H_3R$ and $R'\underline{C}H_2R$, this functionality being found in possible SEI decomposition products lithium ethyl carbonate (LEC), $\underline{C}H_3CH_2OCO_2Li$, lithium butylene dicarbonate (LBDC), $(\underline{C}H_2CH_2OCO_2Li)_2$, and other lithium carbonates. ^1H resonances at approximately 3−5 ppm correlate with overlapping resonances in the carbonate region at ∼161−159 ppm (Figure 7c) including an EC contribution and shoulder at 161 ppm assigned to $RO\underline{C}O_2Li$ (this latter resonance was shown to correlate with $\underline{C}H_2O$ resonances in the homonuclear correlation experiment, Figure 6, and is also

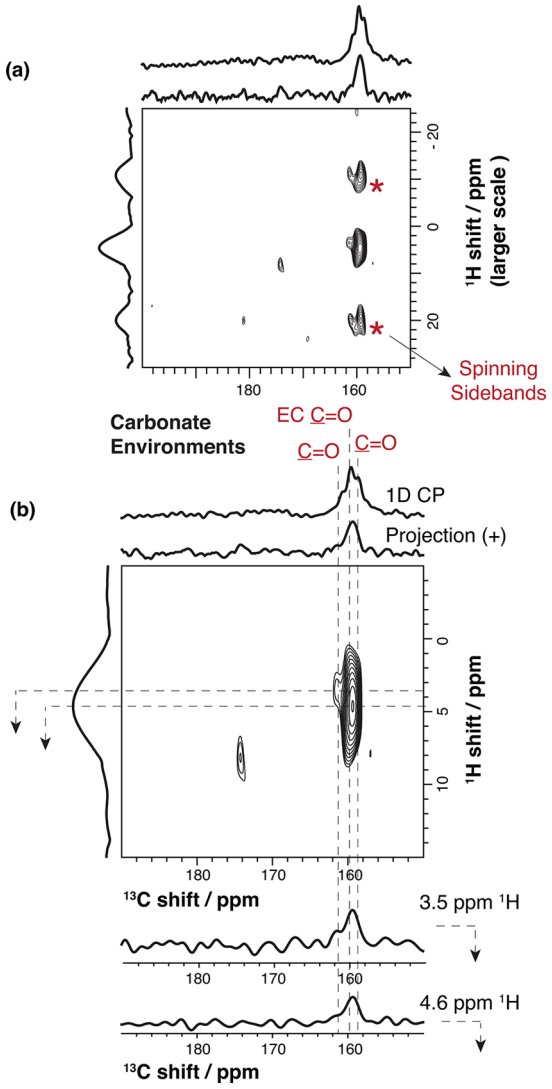

Figure 8. $^1H-^{13}C$ Heteronuclear correlation of a sample prepared with $^{13}C_1$ EC labeled electrolyte. Panel (a) shows the spectrum of panel (b) on a larger ^1H scale to show the ssNMR sidebands confirming multiple environments. The spectrum was acquired on a 700 MHz spectrometer with 10 kHz MAS rate and contact time of 500 μs to transfer magnetization from ^1H to ^{13}C. See Supporting Information for the full spectrum.

confirmed in the $^1H-^{13}C$ correlation spectrum, Figure 8). This 3−5 ppm proton region also correlates with ^{13}C resonances at 62−64 ppm (Figure 7d) (these resonances are consistent with the homonuclear correlation experiment, Figure 6b, which can be assigned to $-O\underline{C}H_2\underline{C}H_2O-$ and $CH_3\underline{C}H_2O-$). These fragments are found in SEI decomposition products such as lithium ethylene dicarbonate (LEDC), $(CH_2OCO_2Li)_2$, LBDC, PEO, and LEC.

The spectrum of the sample prepared with single-label $^{13}C_1$ EC (Figure 8) similarly contains overlapping carbonate environments. The spectrum was acquired at higher field and under different experimental conditions, improving resolution (compared to Figure 7c). The shoulder at 161 ppm, assigned to $RO\underline{C}O_2Li$, correlates with a proton environment at approximately 3.5 ppm. The EC resonance at 160 ppm and shoulder at 159 ppm correlate with ^1H resonances at approximately 4.6 ppm. The 159 ppm shoulder appears to correlate with a larger range of ^1H resonances than the 161 ppm shoulder, indicating

DOI: 10.1021/acs.chemmater.5b04408
Chem. Mater. 2016, 28, 385−398

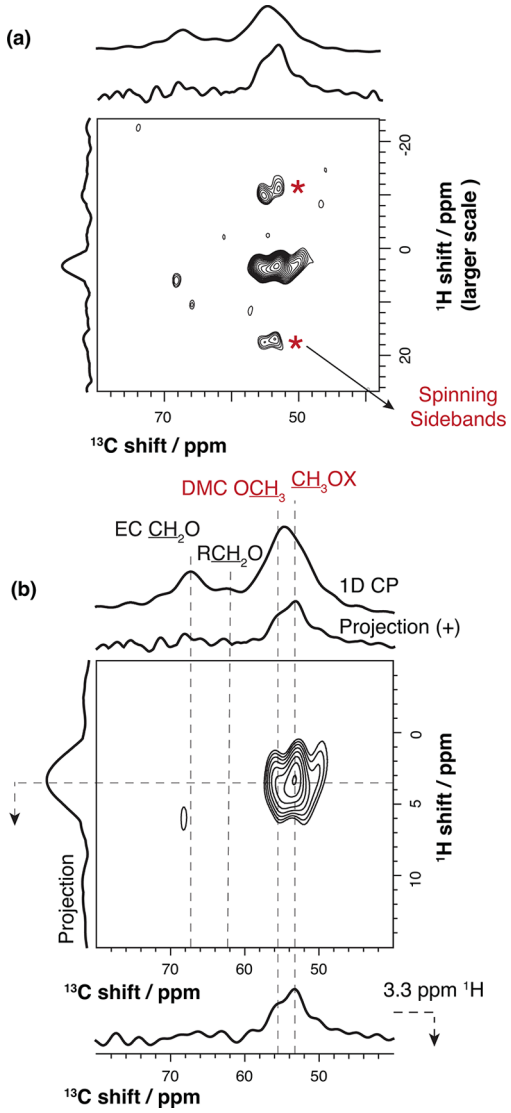

Figure 9. ^{1}H−^{13}C Heteronuclear correlation of a sample prepared with $^{13}C_3$ DMC labeled electrolyte. Panel (a) shows the enlarged spectrum of panel (b) to show the ssNMR sidebands confirming multiple environments. The spectrum was acquired on a 700 MHz spectrometer with 10 kHz MAS rate and contact time of 500 μs to transfer magnetization from ^{1}H to ^{13}C. See Supporting Information for the full spectrum.

either an $ROCO_2Li$ decomposition product with multiple ^{1}H environments, a superposition of $ROCO_2Li$ decomposition products, and/or different EC packing arrangements.

Finally, in the sample prepared with $^{13}C_3$ DMC (Figure 9), a correlation between a resonance at approximately 53 ppm and a ^{1}H resonance at approximately 3.3 ppm (shown in slice, b) can be identified. This correlation is assigned to a $\underline{CH}_3OX$ group; its ^{13}C resonance was also detected in the ^{7}Li−^{13}C CP experiment (Figure 5C-iii). The fragment is found in the SEI decomposition product lithium methyl carbonate (LMC), $\underline{CH}_3OCO_2Li$. A weak shoulder at 49 ppm correlating with ^{1}H at slightly higher field, approximately 2.5 ppm, may indicate a third carbon environment. However, with the absence of a third pair of ssNMR spinning sidebands (see Figure 9a), the presence of an additional species cannot be supported. Finally, correlations from natural abundance EC and its associated decomposition products (^{13}C at 67 and 62 ppm), already examined in the EC-labeled samples, and residual enriched DMC (^{13}C at 56 ppm, ^{1}H at 3.7 ppm) are detected.

Quantification and Proposed Assignment. After identifying functional carbon groups in the SEI, we can now connect the various fragments and obtain assignments and a compositional map of the organic phases. We first provide assignments and then discuss the potential mechanisms by which they form. Integrated intensities of direct excitation ^{13}C spectra are used to quantify the relative contributions of the chemical environments and guide the assignments (Figure 10, Table 2). The detailed analysis is provided in the Supporting Information. As a part of our quantification analysis, we have included experiments with different drying times and DMC-

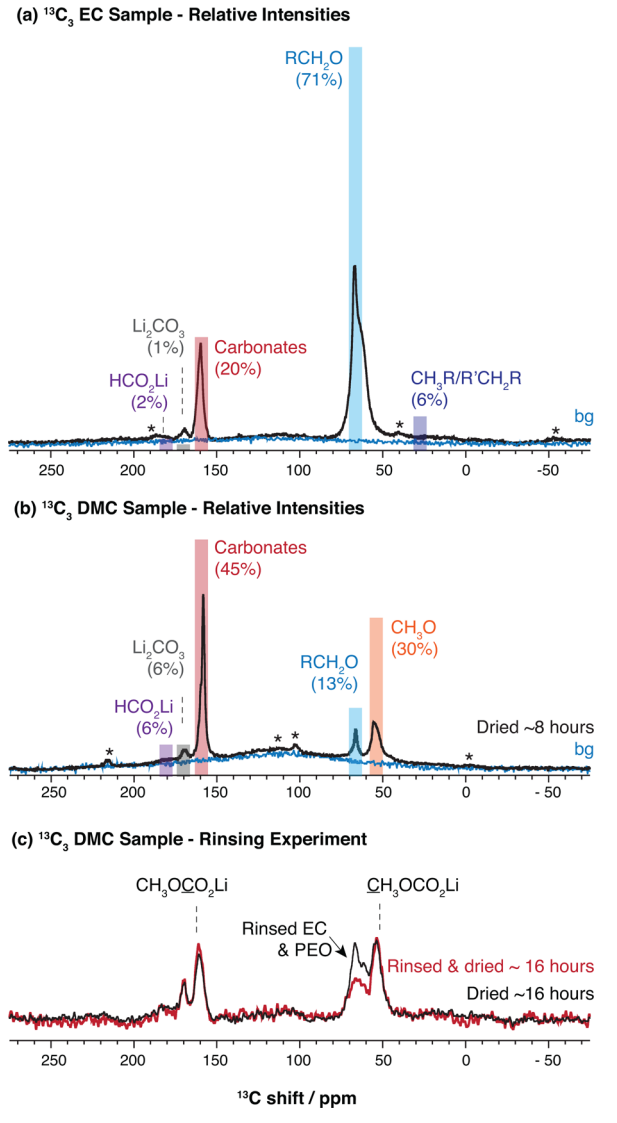

Figure 10. ^{13}C direct excitation spectra of samples prepared using (a) $^{13}C_3$ EC and (b, c) $^{13}C_3$ DMC labeled electrolytes. Relative intensities of the carbon functionalities contained in SEI decomposition products for each sample were determined by peak fitting (see Supporting Information). Spectrum (a) was acquired using a 400 MHz spectrometer with 12 kHz MAS rate and recycle interval of 25 s. Spectra (b, c) were acquired using a 700 MHz spectrometer with 10 kHz MAS rate and recycle interval of 60 s. The background signal of the probes (in blue) are denoted bg (a, b).

DOI: 10.1021/acs.chemmater.5b04408
Chem. Mater. 2016, 28, 385−398

Table 2. Proposed ^{13}C Assignment of EC and DMC SEI Decomposition Products, Based on the Relative Ratios of Their Fragments Observed (Figure 10a,b) Combined with the Results of the ssNMR Correlation Experiments[a]

proposed SEI composition	relative signal (%)	molecular ratio
(a) $^{13}C_3$ EC Sample		
PEO − O$\underline{C}H_2\underline{C}H_2$O−	51	25
LEDC ($\underline{C}H_2O\underline{C}_2Li)_2$	28	7
LEC $\underline{C}H_3\underline{C}H_2O\underline{C}O_2Li$ and LBDC ($\underline{C}H_2\underline{C}H_2O\underline{C}O_2Li)_2$	18	3−6
H$\underline{C}O_2Li$	2	2
$Li_2\underline{C}O_3$	1	1
(b) $^{13}C_3$ DMC Sample		
LMC $\underline{C}H_3O\underline{C}O_2Li$	60	30
nonlabeled EC and products	28	
H$\underline{C}O_2Li$	6	6
$Li_2\underline{C}O_3$	6	6

[a]The relative signal sums to 100% in each sample and takes into account the contribution from all carbons in each molecule.

rinsing in our sample preparation to observe the effect on the detected chemical environments.

(a). $^{13}C_3$ EC Sample. In the direct excitation experiment on the EC-labeled sample, Figure 10a, the broad resonance extending from 0 to 50 ppm contributes approximately 6% of the relative signal intensity and is consistent with functional groups in theoretically predicted SEI products $\underline{C}H_3CH_2OCO_2Li$ (LEC) and ($\underline{C}H_2CH_2OCO_2Li)_2$ (LBDC). Additional oligomeric species including $\underline{R}CO_2Li$ may also contribute to the relative signal intensity in small quantities. LEC and LBDC therefore contribute together to the signal in this region summing up to 6% of the total signal intensity. These species then contribute up to 6% of the signal intensity in the carbonate region. With minor amounts of EC remaining in the sample, the residual 14% signal intensity in the carbonate region is largely attributed to LEDC which also contributes up to 14% relative intensity in the RCH_2O region. From the relative intensity ratio between the RCH_2O and carbonate regions, PEO-type oligomers $(-CH_2-CH_2-O-)_n$, not containing carbonates, are the most dominant contributor to the SEI composition in the sample (also identified in the $^{13}C-^{13}C$ experiment, Figure 6). Finally, we have detected Li_2CO_3 (170 ppm) and RCO_2Li (185 ppm) in a low relative abundance (1% and 2%). With the detection of some HCO_2Li (Figure 7b), the contribution of RCO_2Li ($R \neq H$) is minor in this sample.

(b). $^{13}C_3$ DMC Sample. In the direct excitation experiment on the DMC-labeled sample, Figure 10b, the broad resonance in the CH_3 (53−56 ppm) region contributes 30% of the overall signal, with a minor contribution from residual DMC (56 ppm) and the major contribution assigned to a CH_3OCO_2Li (LMC) decomposition product (53 ppm). The latter is also detected in the $^1H-^{13}C$ HETCOR experiment (Figure 9). On the basis of a 30% contribution in the aliphatic region, LMC accounts for 30% of the intensity in the carbonate region. The residual carbonate and RCH_2O signal is assigned to nonlabeled EC and its decomposition products. HCO_2Li and Li_2CO_3 are seen in smaller amounts of 6% each. With nonlabeled EC and its associated decomposition products contributing significantly in the DMC-labeled sample, it follows that DMC decomposition products contribute less than EC decomposition products to the SEI formed in these samples.

(c). Rinsing: $^{13}C_3$ DMC Sample. A careful experiment to determine the amount of residual labeled-DMC (and nonlabeled EC) in the samples was performed. Samples were divided into two, one-half being immediately rinsed with nonlabeled DMC (<5 ppm of H_2O, <1 min) and the other half remaining unrinsed. These samples were then dried for twice the drying time (approximately 16 h instead of 8 h) to remove as much residual solvent as possible. No difference in the ^{13}C spectra relating to the carbonate resonances or CH_3 (55 ppm) resonances were observed, but the resonances at 67 and 62 ppm assigned to EC and PEO-type oligomers were rinsed away or altered resulting in a broadened and reduced signal. These results confirm negligible (labeled) DMC was left in either of the rinsed or unrinsed samples. As any EC rinsed away is expected to have a relative ratio of 1:2 between its carbonate (159 ppm) and CH_2 (67 ppm) resonances, the rinsing experiment suggests negligible EC in the samples and more PEO-type oligomers being rinsed away (PEO-type oligomers which do not contain a carbonate). Furthermore, assuming rinsing has the most impact on the outer layer of the SEI, the result shows evidence that PEO-type oligomers are structurally located on the outer layer of the SEI; a similar conclusion was drawn by Dedryvère et al. in an XPS study where rinsed and unrinsed samples were compared.[17] Finally, increased drying time was associated with an overall shift of the carbonate peak toward 161 ppm, also observed in preliminary experiments of EC-labeled samples. The result suggests the most stable or least volatile decomposition product is associated with the 161 ppm $ROCO_2Li$ carbonate resonance.

DISCUSSION

Likely EC reactions, based on the literature,[7,9,15−21] are summarized in Scheme 1. The most abundant decomposition

Scheme 1. Possible Decomposition Reactions of EC Supported by the ssNMR Results[a]

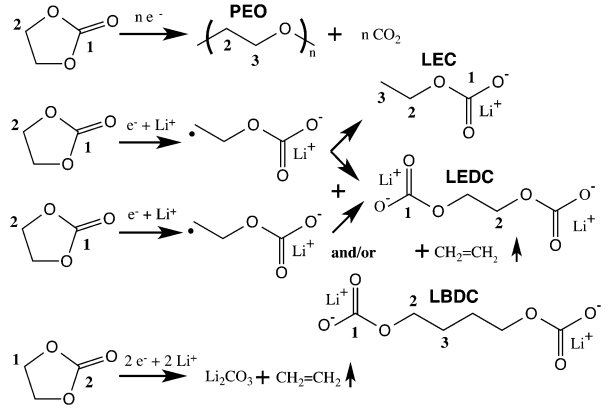

[a]^1H and ^{13}C chemical shifts consistent with the numbered sites 1−3 were observed.

products are PEO-type species with one plausible reaction releasing CO_2. The suggested assignment of EC decomposition products is consistent with a single electron reduction of EC with the ring-opened radical further reacting to form LEC or combining with a second radical to form LBDC. A product with chemical shifts consistent with LEDC was also detected, with one mechanism being the reaction between two EC radicals, CH_2CH_2 being released as gas (and therefore the product is undetected in ssNMR). Li_2CO_3 was also detected in the EC

DOI: 10.1021/acs.chemmater.5b04408
Chem. Mater. 2016, 28, 385−398

labeled systems, with one possible reaction suggested. Additional reactions forming RCO_2Li species in small quantities may also occur.

Likely DMC reactions are summarized in Scheme 2. The suggested assignment of DMC decomposition products

Scheme 2. Possible Decomposition Reactions of DMC Supported by the ssNMR Results[a]

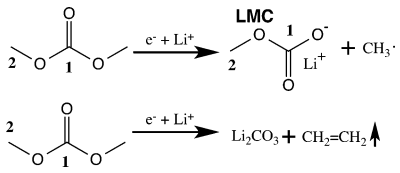

[a] ^1H and ^{13}C chemical shifts consistent with the numbered sites 1−2 were observed.

support a single electron reduction mechanism to form LMC. Li_2CO_3 was also detected in the DMC labeled samples. Additional reactions forming RCO_2Li species in small quantities may also occur.

$LiPF_6$ decomposition leads to LiF, with various decomposition mechanisms proposed in the literature, many of these summarized in a review by Aurbach.[15] Only $LiPF_6$ and LiF were detected by ^{19}F ssNMR (Figure 4b), indicating that PF_x or POF_x, if present, are only there in low concentrations. Furthermore, our results do not show any evidence for C−F species that have previously been detected by XPS in a Si-specific SEI study by Schroder et al.[18] Similarly, we do not find evidence for the SiO_xF_y species found on the surfaces of Si by Philippe et al., as detected by photoelectron spectroscopy within the detection limits of our current experiments.[22] However, our detection of only two ^{19}F resonances is consistent with the results of Delpuech et al., who also investigated the SEI on Si using ^{19}F ssNMR.[28] We note that gas-phase species released from the system during sample preparation may not be detected in the ssNMR measurement, perhaps relevant for the detection of gaseous species such as PF_5 formed in the reaction $LiPF_6 \rightarrow LiF + PF_5$.[15] Trace amounts of water in this system and/or silanol surface groups could also lead to the formation of HF via reactions such as $PF_5 + H_2O \rightarrow PF_3O + 2HF$.[15,45] HF then reacts further with more basic carbonate-containing components of the SEI, for example, $Li_2CO_3 + 2\ HF \rightarrow CO_2 + 2\ LiF + H_2O$[15,17,46] to generate further LiF and water. One possible explanation for the lack of PF_x and POF_x species is that they react further to form PO_x species. Dedryvère et al.[17] have then suggested that these species can attach to the end of the PEO-oligomer chains; ^{31}P NMR studies are, however, required to test this hypothesis.

Overall, the ssNMR quantification results show EC decomposition products are the main contributor to the SEI, with PEO-type oligomers having a significant contribution in the C/Si samples after one electrochemical cycle. DMC decomposition appears to contribute less than EC with its major decomposition product assigned to LMC. The porous nature of the SEI is detected using 2D experiments, with different molecular species correlating with residual solvents. For example, Li salts in the SEI were found to be in close spatial proximity to $LiPF_6$ (Figure 4). The presence of LiF and Li_2CO_3, together with organic species, suggests these components are an integral part of a heterogeneous interface with lithium coordinated to the carbonate environments of $ROCO_2Li$ decomposition products and in inorganic structures. The preliminary rinsing experiments show PEO species are likely located on the outermost layer of the SEI or are more soluble and easily rinsed away in comparison with the semicarbonate $ROCO_2Li$ species.

Our binder-free C/Si system is dry: only trace amounts of water were detected by ^1H NMR in a control experiment (see Supporting Information for more detail). In more practical and typical Si electrode systems cast with binders such as Na-CMC, H_2O or −OH groups will be more prevalent and these electrode systems are more difficult to dry than our binder-free system. Low relative abundances of LiF and Li_2CO_3 were detected here, some authors proposing that they form (or increase in concentration) from the presence of water contamination or air exposure, rather than representing inherent SEI byproducts.[3,15,47] The debate regarding water contamination in ex situ studies leading to the detection of Li_2CO_3 is summarized in a review by Xu.[3] LiOH is also a possible indicator of water contamination.[18,23] Interestingly, no LiOH was detected by ^1H−^7Li NMR (Figure 4). Our results suggest the possibility of Li_2CO_3 being inherent to the SEI formed in these samples rather than detected as an artifact from ex situ experiments and water contamination. However, we note that increases in Li_2CO_3 intensities observed on extended rinsing and/or ambient exposure suggest reactions of the form $(CH_2OCO_2Li)_2 + H_2O \rightarrow Li_2CO_3 + CO_2 + (CH_2OH)_2$ may occur.[15]

By electrochemistry, we have demonstrated the SEI forms on both C and Si surfaces in the electrode (Figure 2). The majority of the SEI formed on the conductive C at 0.8 V (Figure 2c,d) leads to additional capacity (and irreversible capacity) in the first cycle. The much larger capacity loss observed in the C/Si system (Figure 2a,b) demonstrates significant SEI formation is associated with the Si. The growth of the SEI as a function of voltage was monitored by ^1H NMR (Figure 3), our results showing both additional products and increasing quantity as the system approached 1 mV vs Li. Notably, a $CH_3R/R'CH_2R$ resonance, contained in semicarbonate species LEC, LBDC, and RCO_2Li, was clearly distinguishable below 40 mV (see Figures 3 and 7b). Voltage dependent SEI formation has also been observed in other Si systems. For example, a voltage dependence of the SEI composition on Si nanowires in the first electrochemical cycle was also demonstrated by Ruffo et al.[48] Our observed SEI composition may be very different from other studies where different electrochemical cycling was performed. The exact cycling procedure is especially important for Si systems where capacity limited cycling is often used for improved capacity retention, preventing the formation of the $Li_{15}Si_4$ phase to reduce volume expansion in the electrode system.[11,14] As the capacity limitation indirectly reduces the amount of time spent at low voltage in the electrochemical cycling, the chemical composition of the SEI may also differ from our study. Our results strongly imply that any electrochemical cycling alternatives that would reduce the amount of time spent at the long 150 mV plateau of Si in the first electrochemical cycle would have a significant impact on SEI composition. Future ssNMR studies will be performed to explore these phenomena in greater detail.

The DFT chemical shift calculations were an excellent aid in the general understanding of the behavior of the system, being particularly useful in guiding our analysis of the low sensitivity ^{13}C experiments. However, the calculations cannot be used to make definitive assignments, due to several limitations. The

DOI: 10.1021/acs.chemmater.5b04408
Chem. Mater. 2016, 28, 385−398

carbonate chemical shifts of the $ROCO_2Li$ decomposition products were sensitive to the level of convergence and basis set. Complexities such as molecular packing in solid systems are expected to have an impact on chemical shifts.[49] Drying these structures may also have an impact on Li−C distances, with ^{13}C and ^{7}Li chemical shifts sensitive to spatial proximity, particularly relevant to the $ROCO_2Li$ decomposition products. Perhaps most importantly, Li^+ ions may be coordinated to several carbonate groups, resulting in different charge distributions involving carbonate groups from several molecules and a single Li^+ ion, affecting the ssNMR chemical shifts. Interestingly, Borodin et al.[26] has modeled how Li^+ may be coordinated to the carbonates of several LEDC molecules providing a conduction mechanism through the SEI layer. In particular, the DFT calculation results (Tables 1 and S1) show a carbonate resonance systematically higher than expected, indicating the simulated result shows more charge on the carbonates than experimentally detected. Similarly, the Li^+ shifts at 1 ppm are calculated but are more likely near −0.4 ppm based on our experimental observations (Figure 4). DFT calculations show the ^{13}C carbonate shift reducing with distance from a Li^+ ion (Figure 11). Inversely, the calculations

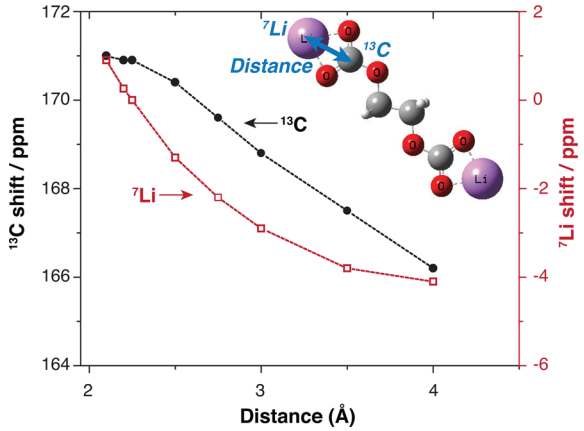

Figure 11. DFT calculations of the chemical shifts of ^{13}C and ^{7}Li with increasing distance between the nuclei (indicated by the blue arrow in the molecule).

demonstrate carbonates with Li^+ in close spatial proximity having a higher chemical shift, as observed experimentally with the 161 ppm $ROCO_2Li$ resonance (Figure 5, inset B-iii).

CONCLUSIONS

A multinuclear ssNMR study using selectively ^{13}C-labeled electrolytes was performed in an effort to understand the composition and structure of the SEI. To aid our assignments of the ^{13}C spectra, chemical shifts of predicted SEI decomposition products were determined. The DFT calculations provided useful trends regarding the chemical shifts, guiding the low sensitivity experiments and assignments. Selective enrichment allowed us to follow the decomposition mechanisms of solvents independently, with EC contributing more significantly to organic decomposition products than DMC. SEI growth was observed by ^{1}H ssNMR as a function of voltage, with electrochemical experiments demonstrating SEI forming on both C and Si surfaces. One consequence of the long lithiation process on Si at approximately 150 mV vs Li is that substantial SEI is formed below this voltage: the Si electrochemistry and cycling voltage limits underlie SEI formation in these systems. The most abundant EC decomposition products detected were PEO-type oligomers, likely on the outermost layer of the SEI. A CH_3R or $R'CH_2R$ environment was formed below 40 mV; while many oligomeric species cannot be ruled out, the experimental results are consistent with an assignment of these carbon functionalities to those present in the theoretically predicted SEI decomposition products LBDC and LEC. RCO_2Li species in low relative abundance were also detected, the majority assigned to HCO_2Li in these samples. $ROCO_2Li$ EC decomposition products were confirmed by correlation experiments, showing a chemical signature consistent with LEDC. The dominant DMC decomposition product contained carbonate and CH_3 resonances in a 1:1 relative abundance and was assigned to LMC. Other species detected in low relative abundance were LiF and Li_2CO_3. The binder-free system allowed for a very dry electrode system, containing minimal water. No LiOH was detected in a 2D $^{1}H-^{7}Li$ correlation experiment. ^{19}F ssNMR showed only LiF and $LiPF_6$, with an absence of PF_x and POF_x type species.

Overall, the experimental data are consistent with an amorphous, porous SEI containing electrolyte. While SEI composition and structure may vary for numerous reasons including electrode formulation, water content, and surface groups, the overall ssNMR strategy employing a multinuclear approach, labeled electrolytes, and 1D and 2D experiments will serve as a method to provide further insight into the structure and composition of this interface on various electrode materials.

ASSOCIATED CONTENT

Supporting Information

The Supporting Information is available free of charge on the ACS Publications website at DOI: 10.1021/acs.chemmater.5b04408.

Chemical shift references (to support our proposed ssNMR assignment); further ssNMR experimental details and spectra (PDF)

AUTHOR INFORMATION

Corresponding Author

*E-mail: cpg27@cam.ac.uk.

Notes

The authors declare no competing financial interest.

ACKNOWLEDGMENTS

This work was partially supported by the Assistant Secretary for Energy Efficiency and Renewable Energy, Office of Vehicle Technologies of the U.S. Department of Energy under Contract No. DE-AC02-05CH11231, under the Batteries for Advanced Transportation Technologies (BATT) Program subcontract #7057154 and by E.I. du Pont de Nemours and Company. A.L.M. is an awardee of a Schiff Foundation Studentship and a nanoDTC Associate. M.L. is an awardee of the Weizmann Institute of Science-National Postdoctoral Award for Advancing Women in Science and thanks the EU Marie Curie intra-European fellowship for funding. We thank Professor D. Wright, C.G.M. Benson, and Dr. Paul Bayley with respect to lab work and advice regarding electrolyte preparation. We thank Dr. Andrew Pell and Dr. John Griffin for discussion regarding NMR pulse sequences. We thank Chris Kerr, Dr. Ken Ogata, and Dr. Elodie Salager with respect to advice and discussion regarding Si electrodes. We thank Dr.

DOI: 10.1021/acs.chemmater.5b04408
Chem. Mater. 2016, 28, 385−398

Rachel Kerber for discussions with respect to DFT calculations. We also thank Dr. Larry Curtiss, Dr. Steve Harris, Dr. William Holstein, and Dr. Elizabeth McCord for discussion regarding the SEI.

REFERENCES

(1) Peled, E.; Golodnitsky, D.; Ardel, G. Advanced Model for Solid Electrolyte Interphase Electrodes in Liquid and Polymer Electrolytes. *J. Electrochem. Soc.* **1997**, *144*, L208−L210.
(2) Winter, M. The Solid Electrolyte Interphase - The Most Important and the Least Understood Solid Electrolyte in Rechargeable Li Batteries. *Z. Phys. Chem.* **2009**, *223*, 1395−1406.
(3) Xu, K. Electrolytes and Interphases in Li-Ion Batteries and Beyond. *Chem. Rev.* **2014**, *114*, 11503−11618.
(4) Aurbach, D.; Gamolsky, K.; Markovsky, B.; Gofer, Y.; Schmidt, M.; Heider, U. On the Use of Vinylene Carbonate (VC) as an Additive to Electrolyte Solutions for Li-ion Batteries. *Electrochim. Acta* **2002**, *47*, 1423−1439.
(5) El Ouatani, L.; Dedryvère, R.; Siret, C.; Biensan, P.; Reynaud, S.; Iratçabal, P.; Gonbeau, D. The Effect of Vinylene Carbonate Additive on Surface Film Formation on Both Electrodes in Li-Ion Batteries. *J. Electrochem. Soc.* **2009**, *156*, A103−A113.
(6) Zhang, S. S. A Review on Electrolyte Additives for Lithium-ion Batteries. *J. Power Sources* **2006**, *162*, 1379−1394.
(7) Nie, M.; Chalasani, D.; Abraham, D. P.; Chen, Y.; Bose, A.; Lucht, B. L. Lithium Ion Battery Graphite Solid Electrolyte Interphase Revealed by Microscopy and Spectroscopy. *J. Phys. Chem. C* **2013**, *117*, 1257−1267.
(8) Ryou, M.-H.; Lee, J.-N.; Lee, D. J.; Kim, W.-K.; Jeong, Y. K.; Choi, J. W.; Park, J.-K.; Lee, Y. M. Effects of Lithium Salts on Thermal Stabilities of Lithium Alkyl Carbonates in SEI Layer. *Electrochim. Acta* **2012**, *83*, 259−263.
(9) Xu, K.; Zhuang, G. V.; Allen, J. L.; Lee, U.; Zhang, S. S.; Ross, P. N.; Jow, T. R. Syntheses and Characterization of Lithium Alkyl Mono- and Dicarbonates as Components of Surface Films in Li-Ion Batteries. *J. Phys. Chem. B* **2006**, *110*, 7708−7719.
(10) Radvanyi, E.; Porcher, W.; De Vito, E.; Montani, A.; Franger, S.; Jouanneau Si Larbi, S. Failure Mechanisms of Nano-Silicon Anodes Upon Cycling: an Electrode Porosity Evolution Model. *Phys. Chem. Chem. Phys.* **2014**, *16*, 17142−17153.
(11) Obrovac, M. N.; Christensen, L. Structural Changes in Silicon Anodes during Lithium Insertion/Extraction. *Electrochem. Solid-State Lett.* **2004**, *7*, A93−A96.
(12) Key, B.; Bhattacharyya, R.; Morcrette, M.; Seznéc, V.; Tarascon, J.-M.; Grey, C. P. Real-Time NMR Investigations of Structural Changes in Silicon Electrodes for Lithium-Ion Batteries. *J. Am. Chem. Soc.* **2009**, *131*, 9239−9249.
(13) Ulldemolins, M.; Le Cras, F.; Pecquenard, B.; Phan, V. P.; Martin, L.; Martinez, H. Investigation on the Part Played by the Solid Electrolyte Interphase on the Electrochemical Performances of the Silicon Electrode for Lithium-ion Batteries. *J. Power Sources* **2012**, *206*, 245−252.
(14) Obrovac, M. N.; Krause, L. J. Reversible Cycling of Crystalline Silicon Powder. *J. Electrochem. Soc.* **2007**, *154*, A103−A108.
(15) Aurbach, D. Review of Selected Electrode-Solution Interactions which Determine the Performance of Li and Li ion Batteries. *J. Power Sources* **2000**, *89*, 206−218.
(16) Aurbach, D.; Zinigrad, E.; Cohen, Y.; Teller, H. A Short Review of Failure Mechanisms of Lithium Metal and Lithiated Graphite Anodes in Liquid Electrolyte Solutions. *Solid State Ionics* **2002**, *148*, 405−416.
(17) Dedryvère, R.; Laruelle, S.; Grugeon, S.; Gireaud, L.; Tarascon, J.-M.; Gonbeau, D. XPS Identification of the Organic and Inorganic Components of the Electrode/Electrolyte Interface Formed on a Metallic Cathode. *J. Electrochem. Soc.* **2005**, *152*, A689−A696.
(18) Schroder, K. W.; Celio, H.; Webb, L. J.; Stevenson, K. J. Examining Solid Electrolyte Interphase Formation on Crystalline Silicon Electrodes: Influence of Electrochemical Preparation and Ambient Exposure Conditions. *J. Phys. Chem. C* **2012**, *116*, 19737−19747.
(19) Tavassol, H.; Buthker, J. W.; Ferguson, G. A.; Curtiss, L. A.; Gewirth, A. A. Solvent Oligomerization during SEI Formation on Model Systems for Li-Ion Battery Anodes. *J. Electrochem. Soc.* **2012**, *159*, A730−A738.
(20) Wang, Y.; Nakamura, S.; Ue, M.; Balbuena, P. B. Theoretical Studies To Understand Surface Chemistry on Carbon Anodes for Lithium-Ion Batteries: Reduction Mechanisms of Ethylene Carbonate. *J. Am. Chem. Soc.* **2001**, *123*, 11708−11718.
(21) Xu, K.; von Cresce, A. Interfacing Electrolytes with Electrodes in Li ion Batteries. *J. Mater. Chem.* **2011**, *21*, 9849−9864.
(22) Philippe, B.; Dedryvère, R.; Gorgoi, M.; Rensmo, H.; Gonbeau, D.; Edström, K. Role of the $LiPF_6$ Salt for the Long-Term Stability of Silicon Electrodes in Li-Ion Batteries - A Photoelectron Spectroscopy Study. *Chem. Mater.* **2013**, *25*, 394−404.
(23) Malmgren, S.; Ciosek, K.; Lindblad, R.; Plogmaker, S.; Kühn, J.; Rensmo, H.; Edström, K.; Hahlin, M. Consequences of Air Exposure on the Lithiated Graphite SEI. *Electrochim. Acta* **2013**, *105*, 83−91.
(24) Lu, P.; Harris, S. J. Lithium Transport Within the Solid Electrolyte Interphase. *Electrochem. Commun.* **2011**, *13*, 1035−1037.
(25) Shi, S.; Lu, P.; Liu, Z.; Qi, Y.; Hector, L. G.; Li, H.; Harris, S. J. Direct Calculation of Li-Ion Transport in the Solid Electrolyte Interphase. *J. Am. Chem. Soc.* **2012**, *134*, 15476−15487.
(26) Borodin, O.; Smith, G. D.; Fan, P. Molecular Dynamics Simulations of Lithium Alkyl Carbonates J. *J. Phys. Chem. B* **2006**, *110*, 22773−22779.
(27) Leifer, N.; Smart, M. C.; Prakash, G. K. S.; Gonzalez, L.; Sanchez, L.; Smith, K. A.; Bhalla, P.; Grey, C. P.; Greenbaum, S. G. ^{13}C Solid State NMR Suggests Unusual Breakdown Products in SEI Formation on Lithium Ion Electrodes. *J. Electrochem. Soc.* **2011**, *158*, A471−A480.
(28) Delpuech, N.; Dupré, N.; Mazouzi, D.; Gaubicher, J.; Moreau, P.; Bridel, J. S.; Guyomard, D.; Lestriez, B. Correlation Between Irreversible Capacity and Electrolyte Solvents Degradation Probed by NMR in Si-Based Negative Electrode of Li-ion Cell. *Electrochem. Commun.* **2013**, *33*, 72−75.
(29) Beattie, S. D.; Larcher, D.; Morcrette, M.; Simon, B.; Tarascon, J.-M. Si Electrodes for Li-Ion Batteries - A New Way to Look at an Old Problem. *J. Electrochem. Soc.* **2008**, *155*, A158−A163.
(30) Magasinski, A.; Zdyrko, B.; Kovalenko, I.; Hertzberg, B.; Burtovyy, R.; Huebner, C. F.; Fuller, T. F.; Luzinov, I.; Yushin, G. Toward Efficient Binders for Li-Ion Battery Si-Based Anodes: Polyacrylic Acid. *ACS Appl. Mater. Interfaces* **2010**, *2*, 3004−3010.
(31) Mazouzi, D.; Lestriez, B.; Roué, L.; Guyomard, D. Silicon Composite Electrode with High Capacity and Long Cycle Life. *Electrochem. Solid-State Lett.* **2009**, *12*, A215−A218.
(32) Nguyen, B. P. N.; Kumar, N. A.; Gaubicher, J.; Duclairoir, F.; Brousse, T.; Crosnier, O.; Dubois, L.; Bidan, G.; Guyomard, D.; Lestriez, B. Nanosilicon-Based Thick Negative Composite Electrodes for Lithium Batteries with Graphene as Conductive Additive. *Adv. Energy Mater.* **2013**, *3*, 1351−1357.
(33) Li, J.; Christensen, L.; Obrovac, M. N.; Hewitt, K. C.; Dahn, J. R. Effect of Heat Treatment on Si Electrodes Using Polyvinylidene Fluoride Binder. *J. Electrochem. Soc.* **2008**, *155*, A234−A238.
(34) Massiot, D.; Fayon, F.; Capron, M.; King, I.; Le Calvé, S.; Alonso, B.; Durand, J.-O.; Bujoli, B.; Gan, Z.; Hoatson, G. Modelling One- and Two-Dimensional Solid-State NMR Spectra. *Magn. Reson. Chem.* **2002**, *40*, 70−76.
(35) Thakur, R. S.; Kurur, N. D.; Madhu, P. K. Swept-Frequency Two-Pulse Phase Modulation for Heteronuclear Dipolar Decoupling in Solid-State NMR. *Chem. Phys. Lett.* **2006**, *426*, 459−463.
(36) Bennett, A. E.; Griffin, R. G.; Ok, J. H.; Vega, S. Chemical Shift Correlation Spectroscopy in Rotating Solids: Radio Frequency-Driven Dipolar Recoupling and Longitudinal Exchange. *J. Chem. Phys.* **1992**, *96*, 8624−8627.
(37) Frisch, M. J.; Trucks, G. W.; Schlegel, H. B.; Scuseria, G. E.; Robb, M. A., Cheeseman, J. R.; Scalmani, G.; Barone, V.; Mennucci,

DOI: 10.1021/acs.chemmater.5b04408
Chem. Mater. 2016, 28, 385−398

B.; Petersson, G. A.; et al. *Gaussian 09*, D.01; Gaussian Inc.: Wallingford CT, 2009.
(38) Becke, A. D. Density-functional Thermochemistry. III. The Role of Exact Exchange. *J. Chem. Phys.* **1993**, *98*, 5648−5652.
(39) Lee, C.; Yang, W.; Parr, R. G. Development of the Colle-Salvetti Correlation-Energy Formula into a Functional of the Electron Density. *Phys. Rev. B: Condens. Matter Mater. Phys.* **1988**, *37*, 785−789.
(40) Frisch, M. J.; Pople, J. A.; Binkley, J. S. Self-Consistent Molecular Orbital Methods 25. Supplementary Functions for Gaussian Basis Sets. *J. Chem. Phys.* **1984**, *80*, 3265−3269.
(41) Krishnan, R.; Binkley, J. S.; Seeger, R.; Pople, J. A. Self-consistent Molecular Orbital Methods. XX. A Basis Set for Correlated Wave Functions. *J. Chem. Phys.* **1980**, *72*, 650−654.
(42) Li, J.; Dahn, J. R. An In Situ X-Ray Diffraction Study of the Reaction of Li with Crystalline Si. *J. Electrochem. Soc.* **2007**, *154*, A156−A161.
(43) Ogata, K.; Salager, E.; Kerr, C. J.; Fraser, A. E.; Ducati, C.; Morris, A. J.; Hofmann, S.; Grey, C. P. Revealing Lithium-Silicide Phase Transformations in Nano-Structured Silicon-Based Lithium Ion Batteries via In Situ NMR Spectroscopy. *Nat. Commun.* **2014**, *5*, 1−11.
(44) Meyer, B. M.; Leifer, N.; Sakamoto, S.; Greenbaum, S. G.; Grey, C. P. High Field Multinuclear NMR Investigation of the SEI Layer in Lithium Rechargeable Batteries. *Electrochem. Solid-State Lett.* **2005**, *8*, A145−A148.
(45) Plakhotnyk, A. V.; Ernst, L.; Schmutzler, R. Hydrolysis in the System $LiPF_6$-Propylene Carbonate-Dimethyl Carbonate-H_2O. *J. Fluorine Chem.* **2005**, *126*, 27−31.
(46) Kanamura, K.; Tamura, H.; Shiraishi, S.; Takehara, Z. I. XPS Analysis for the Lithium Surface Immersed in γ-Butyrolactone Containing Various Salts. *Electrochim. Acta* **1995**, *40*, 913−921.
(47) Edström, K.; Herstedt, M.; Abraham, D. P. A New Look at the Solid Electrolyte Interphase on Graphite Anodes in Li-ion Batteries. *J. Power Sources* **2006**, *153*, 380−384.
(48) Ruffo, R.; Hong, S. S.; Chan, C. K.; Huggins, R. A.; Cui, Y. Impedance Analysis of Silicon Nanowire Lithium Ion Battery Anodes. *J. Phys. Chem. C* **2009**, *113*, 11390−11398.
(49) Yates, J. R.; Pham, T. N.; Pickard, C. J.; Mauri, F.; Amado, A. M.; Gil, A. M.; Brown, S. P. An Investigation of Weak CH···O Hydrogen Bonds in Maltose Anomers by a Combination of Calculation and Experimental Solid-State NMR Spectroscopy. *J. Am. Chem. Soc.* **2005**, *127*, 10216−10220.

DOI: 10.1021/acs.chemmater.5b04408
Chem. Mater. 2016, 28, 385−398